Journal of Sol-Gel Science and Technology (2024) 112:230–239
https://doi.org/10.1007/s10971-024-06512-8

Towards sustainable pest management of broad scope: sol-gel microencapsulation of *Origanum vulgare* essential oil

Giuseppe Angellotti[1] · Cristina Riccucci[2] · Gabriella Di Carlo[2] · Mario Pagliaro[1] · Rosaria Ciriminna[1]

Received: 21 March 2024 / Accepted: 6 August 2024 / Published online: 30 August 2024

Abstract

Showing broad scope pesticidal properties, the *Origanum vulgare* essential oil is highly volatile, limiting effective agricultural applications. Aiming to develop new environmentally friendly and effective biopesticide based on *O. vulgare* essential oil we carried out its template-assisted sol-gel microencapsulation within silica microcapsules. The method affords mesoporous SiO_2 spherical particles about 430 nm in size with uniform size distribution (polydispersion index of 0.184) having encapsulation efficiency up to 13.7 wt%, and large positive zeta potential of 22.8 mV. Dubbed herein "SiliOregan", this new class of sol-gel materials is promising towards the development of solid biopesticides formulated in water for pest management against fungi, insects, bacteria, nematodes, and mites.

Graphical Abstract

Keywords Microencapsulation · Origanum vulgare · Essential oil · Biopesticide · Sol-gel

Highlights

- The development of solid biopesticides formulable in water has substantial practical relevance.
- The high volatility of *Origanum vulgare* essential oil limits agricultural applications.
- We encapsulate *Origanum vulgare* essential oil in silica spherical microcapsules.
- Resulting mesoporous spherical particles are about 430 nm in size with uniform size distribution.
- Large positive zeta potential, encapsulation efficiency up to 13.7 wt% and hydrophilicity of particles are promising.

✉ Mario Pagliaro
mario.pagliaro@cnr.it

✉ Rosaria Ciriminna
rosaria.ciriminna@cnr.it

[1] Istituto per lo Studio dei Materiali Nanostrutturati, CNR, via U. La Malfa 153, 90146 Palermo, Italy

[2] Istituto per lo Studio dei Materiali Nanostrutturati, CNR, via Salaria km 29.3, 00015 Monterotondo, RM, Italy

1 Introduction

Widely used as medicinal plant and culinary herb, oregano (*Origanum*) is an aromatic plant in the mint family Lamiaceae widespread in the Mediterranean region, the Middle East, India, China and in the northern hemisphere [1]. Due to its pronounced ecological adaptability across diverse geographical regions, *O. vulgare* is the most common amid all the species of the genus [1]. Generally extracted from the leaves and flowers (the "aerial part" of the plant), the essential oil (EO) of *Origanum vulgare* is a traditional Chinese medicine (employed for the treatment of heat stroke, fever, vomiting, acute gastroenteritis, and respiratory disorders) [2]. The oil contains plentiful components, though substantial variations in the chemical composition of EOs across countries exist due to the environmental factors that markedly influence its biosynthesis. For example, scholars in China reported that 37 compounds in the EO extracted from leaves and flowers of *O. vulgare* account for ~99% of the total compounds [2]. In the latter EO, carvacrol (~31%), thymol (~19%), *p*-cymene (~11%), and caryophyllene (~8%) were the main components. On the other hand, the EO extracted via hydrodistillation from the leaves of *O. vulgare* growing in the wild of Morocco's Atlas mountains, has durenol (2,3,5,6-tetramethylphenol) as the main component (76%) [3].

Since the late 1990s the EO of *O. vulgare* has been widely studied for its broad scope (fungicide, insecticide, bactericide, nematocide, acaricide) pesticidal properties [4]. However, out of 33 studies published up to 2022 devoted to its insecticidal properties [4], only one reported the outcomes of experiments in the open field. Results, though, were truly promising because the EO at 5% in combination with black soap (60 g/L) killed 92.5% of the carmine cochineal *Dactylopius opuntiae* (Cockerell) females 7 days after application [3]. As recently noted by Jbilou and co-wokers concluding their systematic review on the pesticidal properties of the *O. vulgare* EO [4], its application in agriculture is limited by the high dosages required, due to the high volatility of the oil. Furthermore, the authors noted, very few studies report the effect of the inexpensive aqueous extracts (in place of the EO) [4].

A suitable solution, combining (i) the high pesticidal activity of the EO with, (ii) the ease of processing aqueous formulations and (iii) enhanced activity and reduced volatility allowing reduction of the dosage, lies in the sol-gel microencapsulation of the oil in silica microspheres. First demonstrated with orange essential oil in 2021 [5], this strategy holds large potential for all bioactive EOs, including the substantially cheaper *O. vulgare* EO. In this study we investigate the sol-gel microencapsulation of this bioactive and relatively cheap essential oil within SiO_2 microspheres. Dubbed herein "SiliOregan", this new class of sol-gel materials is promising towards the development of solid biopesticides formulated in water for pest management of broad scope.

2 Materials and methods

2.1 Materials

Tetraethylorthosilicate (TEOS, >99% pure), cetyltrimethylammonium bromide (CTAB, >99% pure), *N*-acetylcysteine (NAC), glycerol, Tween 80, undecane and sodium hydroxide pellets were purchased from Sigma-Aldrich (St. Louis, MI, USA). The essential oil of *O. vulgare* was kindly donated by Esperis (Milan, Italy). All chemicals and solvents were of high purity and were used without any further purification.

2.2 Preparation of the microemulsions

The EO (0.6 mL) was emulsified with an aqueous phase comprising water (20 mL), glycerol (10%, w/v), NAC (0.1%, w/v) using CTAB and Tween 80 as surfactants, both at 1% (w/v) concentration. The mixture was homogenized using a T25 Ultraturrax disperser (IKA-Werke, Staufen, Germany) at 19,000 rpm for 1 min. The resulting emulsion was then placed in an ice-bath and sonicated with a Sonopuls HD 4100 sonicator (Bandelin electronic, Berlin, Germany) for 10 min at 30% amplitude and in pulse condition (Route A).

In a parallel fashion (Route B), a similar microemulsion was prepared adding 1.6 mL of TEOS to EO before the homogenization with aqueous phase as described above. In both cases before the preparation of emulsions the aqueous phase was added with NAC in order to preserve the antioxidant characteristic and avoid degradation phenomena of EO components during the microencapsulation process.

Each resulting microemulsion was ten-fold diluted with distilled water and analysed by a dynamic light scattering (DLS) using a Malvern Zetasizer Nano ZS (Malvern Panalytical, Malvern, Great Britain) equipped with a He-Ne laser at a power of 4.0 mW operating at a wavelength of 633 nm. The measurements were repeated after 24 h sample storage in the dark at room temperature. The analysis was performed in triplicate and results reported as means ± SD (standard deviation).

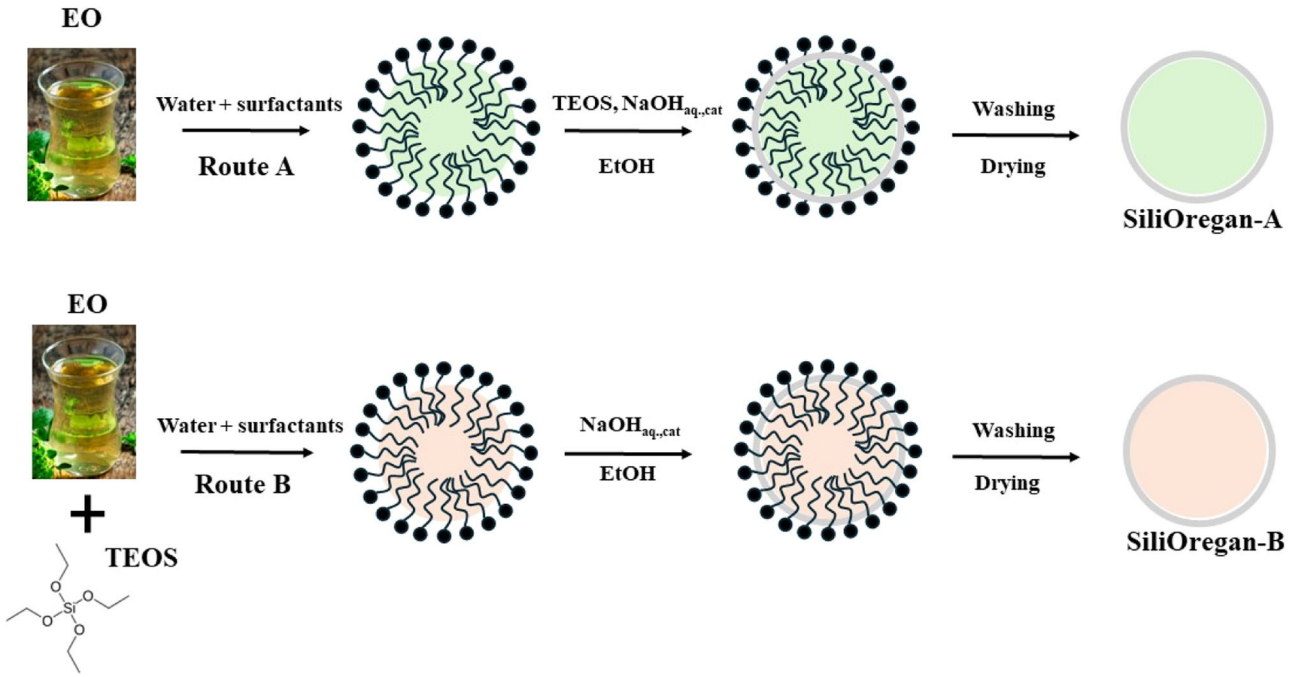

Scheme 1 Sol-gel routes to the SiliOregan capsules: A in which TEOS is added after the emulsion formation; and B in which TEOS is dissolved in the *Origanum vulgare* EO

2.3 Preparation of the microcapsules

The SiliOregan microcapsules were prepared according to Scheme 1.

The microemulsion obtained with "Route A" method was transferred into a round flask kept in an oil bath thermostated at 40 °C, followed by slow addition of TEOS (1.6 mL), EtOH (5 mL), and aqueous NaOH (0.5 mL, 1 N) under continuous stirring. After 48 h a white precipitate (SiliOregan-A) was obtained. The material was recovered by filtration, washed four times (three times with 40% aqueous ethanol, followed by an additional washing step with ultrapure water). After each washing cycle, the supernatant underwent centrifugation at 10,000 rpm for 30 min. Finally, all the microcapsules were recovered through filtration and subsequently dried in an oven at 35 °C for 3 h. A second batch of silica microcapsules (SiliOregan-B) was synthesized in the same manner adding to the microemulsion obtained by the "Route B" aqueous NaOH and EtOH. Blank samples prepared without EO (Empty-A for SiliOregan-A and Empty-B for SiliOregan-B) were also prepared, following the above methods and using *n*-hexane as the oil phase.

2.4 Characterization of the microcapsules

The particle size and zeta-potential of the microcapsules were assessed via DLS using the parameters for particle size determination mentioned above. A sample of the material (5 mg) was dispersed in ultrapure water (1 mL) with the assistance of a sonicator bath. Blank measurements of the aqueous phase containing the surfactants without the SiliOregan capsules were conducted as a control. Each analysis was replicated three times for each prepared batch. The results are presented as means ± SD. The morphology and surface characteristic of the prepared silica microcapsules was performed by scanning electron microscopy using a Zeiss LEO 1530 (Carl Zeiss NTS, Oberkochen, Germany) high-resolution electronic field emission scanning microscope (FE-SEM) with an accelerating voltage of 20 kV.

The TGA/DSC analysis was performed with Mettler Toledo TGA/DSC on a sample of approximately 10 mg using a temperature ramp from 25 °C to about 1000 °C at 10 °C/min under a nitrogen flow. The X-ray diffraction (XRD) measurements were obtained using a D5005 X-ray diffractometer (Bruker AXS, Karlsruhe, Germany) operating at 40 kV and 30 mA. The diffraction profile was obtained at a 0.15°/min acquisition rate, spanning a 10.0°–80.0° 2θ range. The X-ray radiation, generated through a copper (Kα) anode, was rendered monochromatic via the instrument's secondary monochromator.

To assess the load of EO within the microcapsules, two distinct methods were employed. In one method, we dispersed the microcapsules in 2 mL acetonitrile and left the suspension under magnetic stirring for 1 h, after which the suspension was filtered through a 0.45 µm Whatman paper filter, followed by proper dilution with acetonitrile. For each

sample, 1 mL was combined with 20 µL of a 5 µg/mL undecane solution and analyzed using a gas chromatograph equipped with flame ionization detector, to quantify thymol and carvacrol, using their respective calibration curves. The encapsulation efficiency (EE%) was calculated according to Eq. 1:

$$EE\% = \left(\frac{W_t \, or \, W_C}{W_{os}}\right) x100 \quad (1)$$

where W_t and W_c are the amounts of thymol and carvacrol, respectively, while W_{os} is the weight of microcapsules.

In another route, samples of the solution of extracted EO in acetonitrile were analyzed using a UV-Vis spectrophotometer operated at 280 nm. The quantification process was executed employing a previously constructed calibration curve. The EO encapsulation percentage (EO %) was calculated according to Eq. 2:

$$EO\% = \left(\frac{W_{eo}}{W_{os}}\right) x100 \quad (2)$$

where W_{eo} is the amount of *O. vulgare* EO contained in each sample. The analysis was performed in triplicate and the results expressed as means ± SD. FTIR spectra were acquired using a Bruker Vertex Advanced Research Fourier Transform Infrared spectrometer (Bruker, Billerica, MA, USA) spanning the 400–4000 cm^{-1} range, with a lateral resolution of 2 cm^{-1} and 128 scans. Approximately 5 mg of each microcapsule was homogenously mixed with 100 mg of ultrapure KBr (FT-IR grade, ≥99% pure, Sigma-Aldrich) using a pestle and mortar to form a consistent mixture. Subsequently, a Specac Mini-Pellet laboratory hydraulic press was employed to prepare pellets, applying a 12 t weight for 5 min. For the pure EO, the IR spectra were obtained using the attenuated total reflection (ATR) sampling technique using the same spectrometer, equipped with a Transit Platinum ATR probe and a diamond crystal. The measurements were conducted within the 600–4000 cm^{-1} range, with a lateral resolution of 2 cm^{-1} and 128 scans.

The specific surface area (SSA), pore specific volume (PSV) and pore size distribution of the microcapsules were assessed from the adsorption-desorption N_2 isotherms using the NOVA 2000e surface area and pore size analyzer (Quantachrome, Boynton Beach, FL, USA) with cryogenic N_2 as the adsorbate. Prior to analysis, the microcapsule samples underwent degassing under vacuum at approximately 30 °C overnight. The SSA of the samples was determined utilizing the multipoint Brunauer-Emmett-Teller (BET) model, employing the average adsorption and desorption values of P/P_o within the range of 0–0.98 atm at the fixed temperature of 77.4 K. The pore size distribution and PSV were calculated by applying the Barrett-Joyner-Halenda (BJH) model to the desorption branch of the isotherms across all P/P_o ranges.

2.5 GC-FID and UV-Vis analyses

The assessment of thymol and carvacrol concentration was carried out using a Shimadzu GC-FID 17 A gas chromatograph with a 50–250 °C a temperature range of using a ramp rate of 10 °C/min. The GC was equipped with a flame ionization detector (FID) for compound detection. The chromatographic separation utilized a Supelco SPB-1701 capillary column (Supelco, Bellefonte, PA, USA). For the quantitative determination of the target compounds, calibration curves were constructed. Standard solutions with known concentrations in acetonitrile were prepared. These solutions, containing the internal standard undecane, were injected into the GC-FID using an injection syringe. Calibration curves were obtained by plotting the ratio between the signal of thymol or carvacrol and undecane against the corresponding concentrations of analytes. The parameters of the respective calibration curves were as follows:

Thymol: Concentration range: 0.013–0.257 mg/mL; retention time: 14.85 min; Equation: $y = 0.0469 + 10.72x$ [signal-ratio thymol/undecane; ($R^2 = 0.999$)].

Carvacrol: Concentration range: 0.014–281 mg/mL; retention time: 15.10 min; Equation: $y = 0.0723 + 12.016x$ [signal-ratio carvacrol/undecane; ($R^2 = 0.999$)].

The UV-Vis measurements were carried out using a Shimadzu UV-1800 spectrophotometer (Shimadzu, Kyoto, Japan). Calibration curves were constructed by preparing a series of standard solutions containing known concentrations of EO in acetonitrile, measuring the absorbance values at 274 nm. A blank analysis conducted using an acetonitrile-based extract of empty silica microcapsules, revealed no detectable peaks, confirming the absence of interference with other components. The calibration curve was constructed by plotting the absorbance values against the corresponding concentrations of the standard solutions in the 0.005-0.1 mg/mL oil concentration range. The linear equation: $y = -0.0027 + 11.588x$ [mg/mL, ($R^2 = 0.999$)].

2.6 Data analysis

Data were expressed as means ± SD. The experimental data and graph were processed using OriginPro (OriginLab, Northampton, MA, USA) as software.

3 Results and discussion

The results of the DLS analysis of the microemulsions in Table 1 in terms of colloidal particle size and polydispersity index (PDI) show no substantial differences

Table 1 Size (D) and polydispersity index (PDI) of the prepared microemulsions right after preparation (0 h) and after 24 h storage

Sample	D (nm)		PDI	
	0 h	24 h	0 h	24 h
Emulsion A	172 ± 72	316.9 ± 195	0.192	0.417
Emulsion B	208.9 ± 64	391.2 ± 256	0.094	0.458

Table 2 Size, polydispersity index and ζ potential of the SiliOregan microcapsules

Sample	D (nm)	PDI	ζ potential (mV)
SiliOregan-A	459.1 ± 147	0.433	32.5 ± 7.5
SiliOregan-B	426.9 ± 109	0.184	22.8 ± 5.7

between the microemulsions prepared via the two different routes A and B.

In both cases, microemulsions with droplets diameter below 250 nm were obtained. These dimensions nearly doubled after 24 h of static storage, and the standard deviation increased. Importantly, however, the micelle growth did not impact the size distribution, which remained homogeneous as shown by the PDI values below 0.5. Results in Table 2 show that the sol-gel silica microcapsules resulting from the two sol-gel routes, SiliOregan-A and SiliOregan-B, were not significantly different in terms of size and ζ potential.

In both instances, a homogeneous dispersion was achieved with PDI values below 1.003, a threshold considered critical for determining poly- and monodisperse systems (particles are considered monodisperse if their PDI < 1.003) [6].

Showing evidence of successful EO microencapsulation, the particle size of the SiliOregan microspheres was slightly higher than the size of the precursor microemulsion droplets (the "microreactor" of the sol-gel synthesis route) due to size of the SiO_2 shell encapsulating the oil inside the silica microcapsules, due to sol-gel polycondensation of the silane precursors around the oil droplets [7]. The large positive values of the ζ potential were likely due to the cationic surfactant CTAB molecules partly remaining entrapped at the outer surface of the silica microcapsules [7]. Such large values of the ζ electrokinetic potential in colloidal dispersion impart stability to colloidal dispersions as Coulombic charge repulsion hinders particle aggregation, regardless of the high surface reactivity of the SiO_2 microspheres containing plentiful silanol groups at the surface [8].

The FE-SEM photographs in Fig. 1 clearly reveal the morphology differences between SiliOregan-A and SiliOregan-B microcapsules. In the former case, the spherical particles are tightly aggregated. In contrast, the SiliOregan-B microcapsules (and the corresponding blank capsules Empty-B) exhibit a spherical shape and a regular size distribution, without the evident cluster condensation noted in SiliOregan-A.

In all cases the particle size of the microcapsules identified by the SEM analysis is smaller (≃ 200 nm) than the results obtained by DLS because the latter technique measures intensity distributions and has low size resolution, due to the reduced scattering of light of the smaller particle sizes [9].

The structural difference is reflected also in the higher microencapsulation efficiency of SiliOregan-B compared to the SiliOregan-A with respect to the overall amount of EO encapsulated and with reference to the two main components of *O. vulgare* essential oil thymol and carvacrol (Table 3).

In the case of SiliOregan-B, TEOS is dissolved in the EO, and both are smoothly emulsified with the aqueous phase. In the case of SiliOregan-A, TEOS is added after the emulsion formation, along with EtOH and NaOH. As a result, the hydrolytic polycondensation at the O/W interface of the microemulsion results in the formation of a SiO_2 shell that is less effective in encapsulating the oil. Furthermore, the ethanol co-solvent partly dissolves and removes the EO from the core of the O/W micelle.

In both A and B microencapsulation routes, though, the amount of EO microencapsulated exceeds 11% by weight, in line with the amount of EO microencapsulated in the case of other spherical sol-gel microcapsules such as those doped with orange oil [5]. In detail, the 11.34 wt% load for Route A and 13.7% for Route B payloads are significantly lower than encapsulation efficiency values up to 33.9%, when encapsulating the same EO using spray drying using maltodextrin, Arabic gum, and modified starch as shell materials [10]. However, spray drying microencapsulation is completely different from sol-gel microencapsulation in core-shell SiO_2 microspheres [7]. In the former case, readily hydrolysable polysaccharides form an irregular matrix with the dopant molecules comprising the EO ending dispersed at the outer surface of the material. In the case of the sol-gel microencapsulation, a true core comprised of the EO is surrounded by a spherical shell of glassy silica (Fig. 1) that stabilizes, chemically and physically, the organic molecules comprising the oily core [7].

The morphology difference noted via the SEM analysis can be attributed to instability during the sol-gel nucleation process, where interactions between microcapsules lead to condensation and the formation of irregular structure.

The type IV adsorption-desorption isotherm of SiliOregan-B and the blank material (Empty-B) (Fig. 2, top) are typical of mesoporous materials consisting of

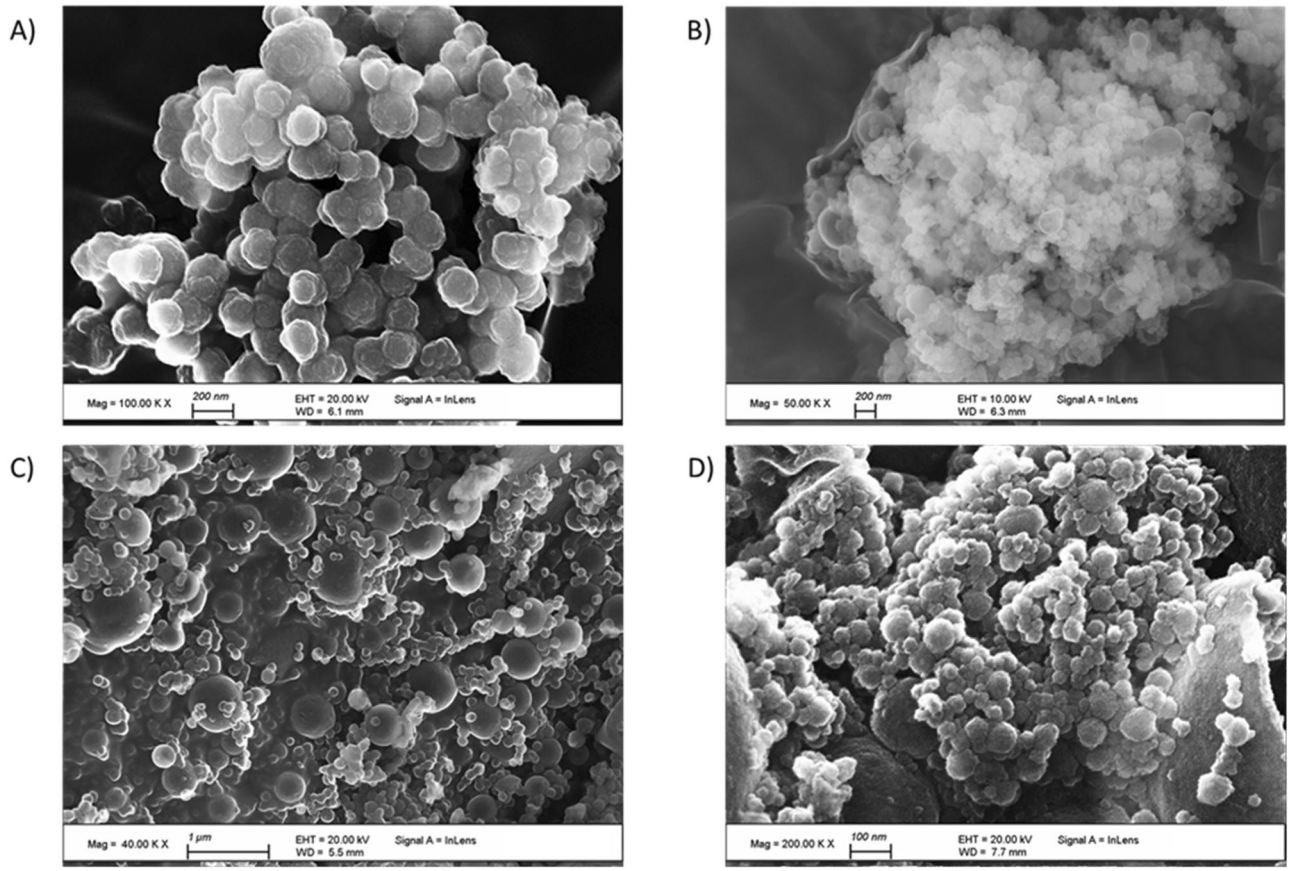

Fig. 1 SEM images of SiliOregan-A and SiliOregan-B microparticles (top, **A** and **B** photographs, respectively). SEM images of the corresponding Empty-A and Empty-B blank microparticles (bottom, **C** and **D** photographs, respectively)

Table 3 Amount of oil, thymol and carvacrol entrapped in the SiliOregan samples

Sample	EE% (thymol)	EE% (carvacrol)	OE%
SiliOregan-A	3.57 ± 0.48	3.83 ± 0.52	11.34 ± 1.09
SiliOregan-B	4.89 ± 0.25	5.33 ± 0.28	13.7 ± 0.4

agglomerates of spheroidal particles of relatively uniform size and dispersion [11, 12]. Successful entrapment of EO is shown by the substantial reduction (Table 4) of the pore specific volume (PSV, from 1.33 to 0.66 cm^3/g) and specific surface area (SSA, from ~310 to ~120 m^2/g).

Indirect evidence of the "outbound" polycondensation mechanism of TEOS taking place at the O/W micelle interface, with the solvent action of EtOH molecules, is suggested by the four-fold reduction in SSA going from SiliOregan-B (~120 m^2/g) to SiliOregan-A (~34 m^2/g). Indeed, devoid of added EO, the blank version (Empty-A) has high (~228 m^2/g) and large SPV (0.75 cm^3/g).

The FT-IR spectrum (Fig. 3) of the *O. vulgare* EO includes the peaks at 811, 994, 1116, 1173, 1251 cm^{-1} of its main component carvacrol alongside the signals at 2959 cm^{-1} corresponding to CH symmetric and antisymmetric stretching vibration modes and at 3386 cm^{-1} ascribed to the OH stretching mode in both thymol and carvacrol [13].

The FTIR spectra of both empty and doped silica microcapsules are dominated by the typical stretching and bending vibrations of the Si–O–Si and Si–O group peaks at 1100 cm^{-1} and 797 cm^{-1}, as well as by the broad peak in the 3500–3200 cm^{-} due to the stretching of the OH group of the silanol groups. The weak signal at 2959 cm^{-1}, absent in the corresponding empty microcapsules, but discernible in the spectra of both microencapsulant materials SilOregan-A and SilOregan-B, is ascribed to the CH symmetric and antisymmetric stretching vibration modes of carvacrol and thymol present in the EO. Finally, the presence of residual CTAB is unveiled by the bands at 1490, 1478, and 1468 cm^{-1}, assigned to CH_3 and CH_2 deformation modes [14].

The X-ray powder diffraction patterns of SiliOregan-A and SiliOregan-B in Fig. 4 are nearly superimposable. Both are dominated by a broad band at $2\theta = 22–23°$, showing that the materials are amorphous, in full agreement with previous results obtained with sol-gel silica similarly made

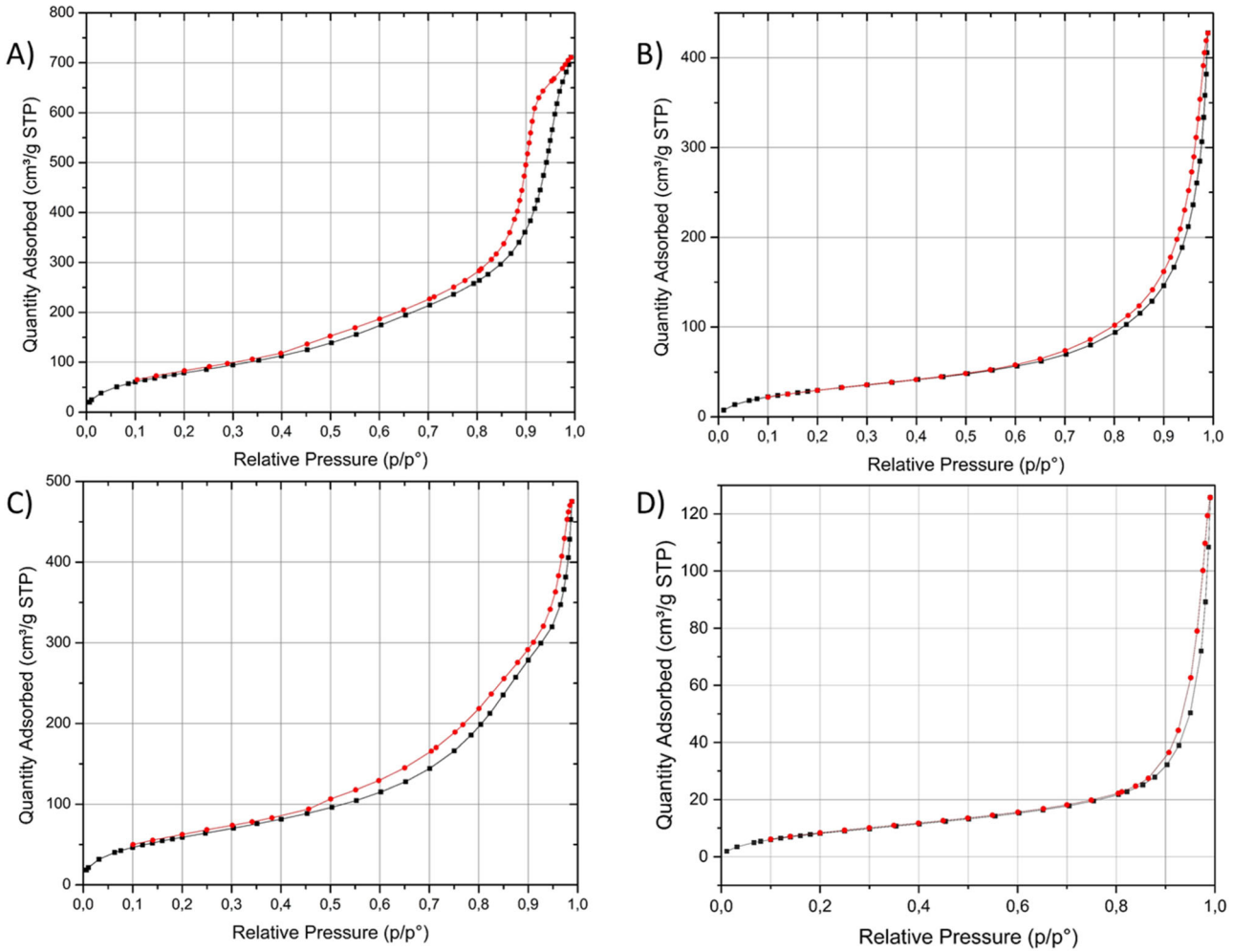

Fig. 2 Top: N_2 adsorption/desorption isotherms of Empty-B **A** and SiliOregan-B **B**. Bottom: N_2 adsorption/desorption isotherms of Empty-A **C** and SiliOregan-A **D**

Table 4 Specific surface area, pore volume and pore size of SiliOregan and corresponding blank materials

Sample	Specific surface area (m^2/g)	Specific pore volume (cm^3/g)	Pore size (nm)
SiliOregan-A	34.01	0.19	22.76
SiliOregan-B	120.25	0.66	19.41
Empty-A	228.24	0.75	10.53
Empty-B	309.83	1.33	10.79

with both CTAB and Tween 80 as templates subsequently dried at low temperature (55 °C) [15].

The TGA analysis on empty microparticles (Empty A and Empty B, Fig. 5) shows an initial weight loss at 58 °C ascribed to the volatilization of EtOH residues. Subsequent 18.14% weight loss at 261 °C indicates decomposition of the residual surfactant CTAB molecules entrapped at the outer surface of the microspheres, that mixed with silica particles degrade at about 268 °C [16]. Finally, the significant weight loss at over 430 °C is ascribed to the decomposition of the organic species residual of CTAB decomposition, with concurrent condensation of silanol groups, leading to the formation of a closed SiO_2 structure comprised of siloxane Si-O-Si bonds [17].

A similar thermal decomposition pattern was evident in SilOregan-A with a slight shift in temperature at each decomposition stage (Fig. 5, top). Notably, an additional decomposition step at 153 °C with 7.58% weight loss was due to volatilization of certain components from the *O. vulgare* EO, as confirmed by the thermogram of the pure oil which showed a thermal decomposition/evaporation at 160 °C.

The TGA pattern of SiliOregan-B is superimposable with the thermogram of SiliOregan-A (Fig. 5, bottom). A significant shift to higher temperature in degradation phenomena is clearly observed when compared to empty silica microcapsules. The 8.13% weight loss at 153 °C, higher than SiliOregan-A, confirms the better oil encapsulation efficiency of the former material (and corresponding route).

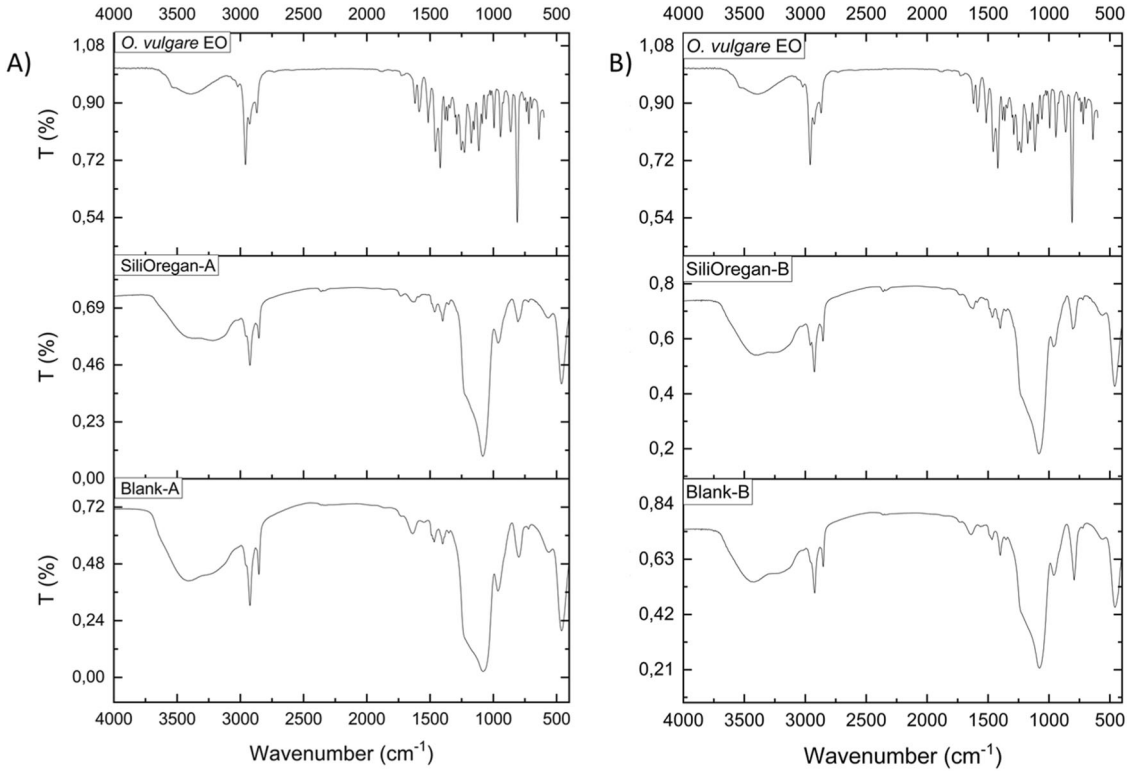

Fig. 3 FT-IR spectra of: **A** *O. vulgare* EO and SiliOregan-A and blank capsules; **B** SiliOregan-B and blank capsules

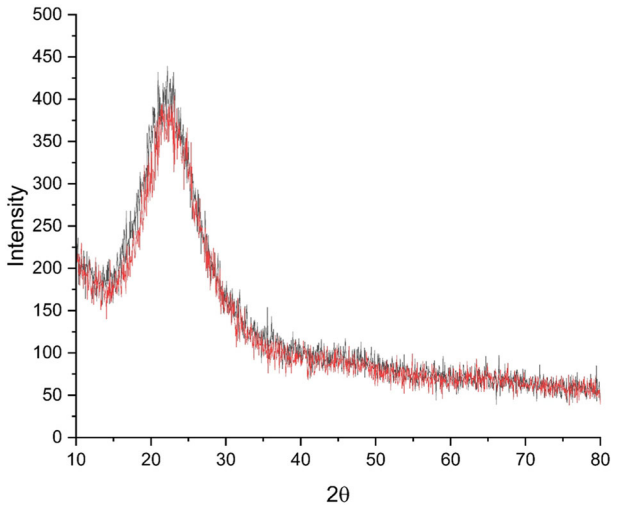

Fig. 4 X-ray diffraction patterns of SiliOregan-A (red curve) and SiliOregan-B (black curve)

4 Conclusions

In conclusion, aiming to develop new environmentally friendly and effective solid biopesticide to be formulated in water, we studied the sol-gel microencapsulation of *Origanum vulgare* essential oil within silica microcapsules obtained via the template-assisted (and highly reproducible) sol-gel route [7]. The most effective route involves dissolving the EO in the precursor TEOS prior to the sol-gel hydrolytic polycondensation of TEOS taking place at the outer surface of the O/W emulsion microdroplets eventually affording the SiO_2 spherical shells encapsulating the oil. The resulting optimal "SiliOregan" material is comprised of amorphous SiO_2 microspheres 427 nm in size with uniform size distribution (polydispersion index of 0.184) encapsulating a substantial load of *O. vulgare* essential oil amounting to nearly 14 (13.7) weight per cent.

The particles, furthermore, are mesoporous with an average pore size of 19.4 nm and a relatively large specific pore volume of 0.66 cm^3/g. Being hydrophilic and exhibiting a high ζ potential of +22.8 mV, this microparticulate material is highly promising towards the development of a truly sustainable (economically and environmentally) biopesticide for pest management of broad scope (against fungi, insects, bacteria, nematodes, and mites) [4]. New research aimed at evaluating the practical applicability of SiliOregan aqueous formulations in collaboration with entomologists is in course. The outcomes will be reported in due time.

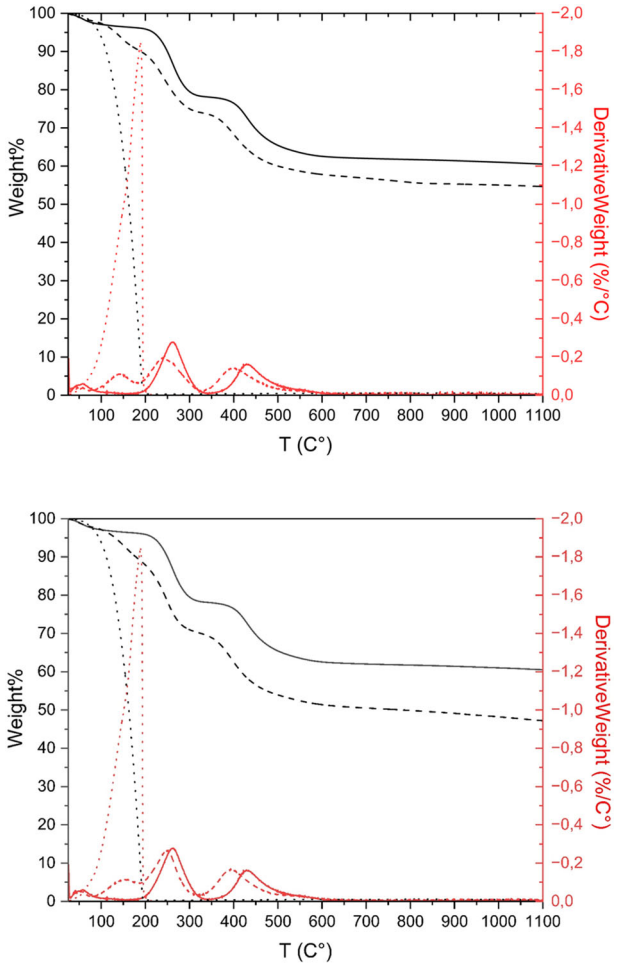

Fig. 5 Top: weight loss percentage (black) and derivative curves (red) of empty (blank) silica microcapsules (straight line), SiliOregan-A (dashed line), and *O. vulgare* EO (dots). Bottom: weight loss percentage (black) and derivative curves (red) of empty silica microcapsules (straight line), SiliOregan-B (dashed line), and *O. vulgare* EO (dots)

Data availability

All data are available upon reasonable request by contacting the corresponding authors.

Acknowledgements We thank Professor Orlando Campolo, University Mediterranea of Reggio Calabria, Italy, for the generous gift of *O. vulgare* essential oil. Thanks to Sara Miceli, undergraduate student at the University of Palermo, for assistance during the material preparations. We thank Dr Francesco Giordano, Dr Giuseppe Pantaleo and Dr Nunzio Gallì, Istituto per lo Studio dei Materiali Nanostrutturati, CNR, for assistance with the XRD, TGA and surface textural analyses, respectively.

Author contributions "R.C. and M.P. conceived the study and wrote the main manuscript text. G.A., G.D.C. and C.R. conducted the material synthesis and characterization experiments. All authors reviewed the manuscript."

Funding This study was funded by European Union NextGenerationEU through the SAMOTHRACE (Sicilian Micro and Nano Technology Research and Innovation Center) Innovation Ecosystem (PNRR – Mission 4 Component 2 - Investment 1.5 (ECS00000022)) - CUP B63C22000620005. Open access funding provided by Consiglio Nazionale Delle Ricerche (CNR) within the CRUI-CARE Agreement.

Compliance with ethical standards

Conflict of interest The authors declare no competing interests.

Publisher's note Springer Nature remains neutral with regard to jurisdictional claims in published maps and institutional affiliations.

References

1. Sharifi-Rad M, Berkay Yılmaz Y, Antika G, Salehi B, Boyunegmez Tumer T, Kulandaisamy Venil C, Das G, Kumar Patra J, Karazhan N, Akram M, Iqbal M, Imran M, Sen S, Acharya K, Dey A, Sharifi-Rad J (2021) Phytochemical constituents, biological activities, and health-promoting effects of the genus *Origanum*. Phytother Res 35:95–121. https://doi.org/10.1002/ptr.6785
2. Han F, Ma G-Q, Yang M, Yan L, Xiong W, Shu JC, Zhao ZD, Xu HL (2017) Chemical composition and antioxidant activities of essential oils from different parts of the oregano. J Zhejiang Univ Sci B 18:79–84. https://doi.org/10.1631/jzus.B1600377
3. Ramdani C, El Fakhouri K, Sbaghi M, Bouharroud R, Boulamtat R, Aasfar A, Mesfioui A, El Bouhssini M (2021) Chemical composition and insecticidal potential of six essential oils from Morocco against *Dactylopius opuntiae* (Cockerell) under field and laboratory conditions. Insects 12:1007. https://doi.org/10.3390/insects12111007
4. Jbilou R, Radice M, Bakrim A, Bouayad N, Rharrabe K (2024) Potential use of *Origanum vulgare* in agricultural pest management control: a systematic review. J Plant Dis Prot 131:347–363. https://doi.org/10.1007/S41348-023-00839-0
5. Sciortino M, Scurria A, Lino C, Pagliaro M, D'Agostino F, Tortorici S, Ricupero M, Biondi A, Zappalà L, Ciriminna R (2021) Silica-microencapsulated orange oil for sustainable pest control. Adv Sust Syst 5:2000280. https://doi.org/10.1002/adsu.202000280
6. De La Vega JC, Elischer P, Schneider T, Häfeli UO (2013) Uniform polymer microspheres: monodispersity criteria, methods of formation and applications. Nanomedicine 8:265–285. https://doi.org/10.2217/nnm.12.210
7. Pagliaro M, Sciortino M, Ciriminna R, Alonzo G, De, Schrijver A (2011) From molecules to systems: sol-gel microencapsulation in

silica-based materials. Chem Rev 111:765–789. https://doi.org/10.1021/cr100161x
8. Vazquez NI, Gonzalez Z, Ferrari B, Castro Y (2017) Synthesis of mesoporous silica nanoparticles by sol-gel as nanocontainer for future drug delivery applications. Bol Soc Esp Ceram V 56:139–145. https://doi.org/10.1016/j.bsecv.2017.03.002
9. Fissan H, Ristig S, Kaminski H, Asbach C, Epple M (2014) Comparison of different characterization methods for nanoparticle dispersions before and after aerosolization. Anal Meth 6:7324–7334. https://doi.org/10.1039/c4ay01203h
10. Alvarenga Botrel D, Vilela Borges S, Victória de Barros Fernandes R, Dantas Viana A, Gomes da Costa MJ, Reginaldo Marques G (2012) Evaluation of spray drying conditions on properties of microencapsulated oregano essential oil. Int J Food Sci Technol 47:2289–2296. https://doi.org/10.1111/j.1365-2621.2012.03100.x
11. Gregg, SJ, Sing, KSW (1982) Adsorption, Surface Area and Porosity, 2nd edn. Academic Press, London; pp. 287.
12. Sing KSW, Everett DH, Haul RAW, Moscou L, Pierotti RA, Rouquérol J, Siemieniewska T (1985) Reporting physisorption data for gas/solid systems with special reference to the determination of surface area and porosity (Recommendations 1984). Pure Appl Chem 57:603–619. https://doi.org/10.1351/pac198557040603
13. Valderrama ACS, Rojas De GC (2017) Traceability of active compounds of essential oils in antimicrobial food packaging using a chemometric method by ATR-FTIR. Am J Anal Chem 8:726–741. https://doi.org/10.4236/ajac.2017.811053
14. Fidalgo A, Ciriminna R, Ilharco LM, Sciortino M, Pagliaro M (2012) Sol-gel microencapsulation of organic molecules: a structural and chemical insight. ChemPlusChem 77:536–540. https://doi.org/10.1002/cplu.201200077
15. Cardinal MF, Lovino M, Bernik DL (2007) Comparative study of the porosity induced by CTAB and Tween as silica templates. Mater Sci Eng C 27:75–79. https://doi.org/10.1016/j.msec.2006.02.007
16. Zhang T, Xu G, Puckette J, Blum FD (2012) Effect of silica on the structure of cetyltrimethylammonium bromide. J Phys Chem C 116:11626–11634. https://doi.org/10.1021/jp303338t
17. Ciriminna R, La Mattina R, Pantaleo G, Pagliaro M (2014) Thermogravimetric Investigation of sol-gel microspheres doped with aqueous glycerol. Sust Chem Proc 2:26. https://doi.org/10.1186/s40508-014-0026-x